Fuel 259 (2020) 116263

Contents lists available at ScienceDirect

Fuel

journal homepage: www.elsevier.com/locate/fuel

Full Length Article

Intrinsic kinetics, thermodynamic parameters and reaction mechanism of non-isothermal degradation of torrefied *Acacia nilotica* using isoconversional methods

Satyansh Singh, Jyoti Prasad Chakraborty*, Monoj Kumar Mondal

Department of Chemical Engineering and Technology, Indian Institute of Technology (Banaras Hindu University), Varanasi 221 005, India

GRAPHICAL ABSTRACT

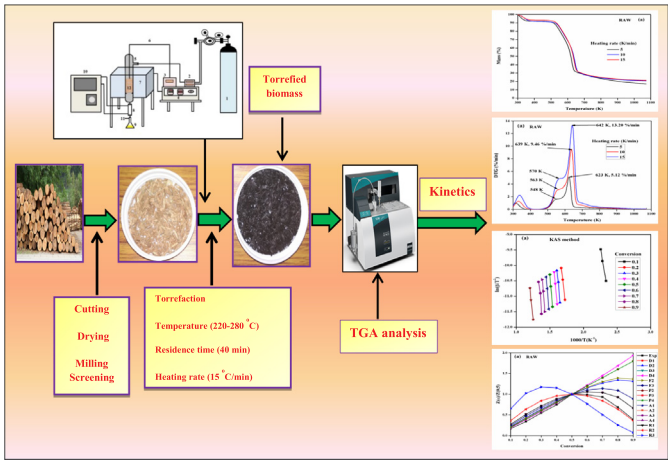

ARTICLE INFO

Keywords:
Acacia nilotica
Torrefaction
Non-isothermal kinetics
Thermodynamic parameter
Reaction mechanism

ABSTRACT

The objective of this work is to examine the suitability of torrefied biomass for bio-energy generation by investigating its physicochemical characteristics, kinetic and thermodynamic parameters as well as reaction mechanism during pyrolysis. Thus, torrefaction of *Acacia nilotica* was performed in a fixed bed reactor at 220, 250 and 280 °C, with constant residence time (40 min) and heating rate (15 °C/min). Pyrolysis of torrefied biomass obtained at 220 °C (T-220), 250 °C (T-250) and 280 °C (T-280) was performed using thermogravimetric analyzer at three different heating rate viz. 5, 10 and 15 K/min. Further, isoconversional models namely, Kissinger-Akahira-Sunose (KAS), Ozawa-Wall-Flynn (OWF), Friedman and Starink were employed to calculate the kinetic parameters (activation energy and pre-exponential factor) of raw and torrefied biomass. Using kinetic parameters obtained from KAS method, thermodynamic parameters (enthalpy, Gibbs free energy, and entropy) were calculated at a heating rate of 10 K/min. The activation energy for raw and T-220, T-250, and T-280 using KAS method were found to be 221.49, 241.58, 185.06, and 121.83 kJ/mol, respectively. The increase in activation energy of T-220 might be due to a higher percentage of cellulose content in it than raw biomass. Reaction mechanism during pyrolysis of raw and torrefied biomass was predicted using Criado method (Z-master plot). For raw biomass and T-220, diffusion models were followed; however, for T-250 and T-280, random nucleation

* Corresponding author.
E-mail address: jpc.che@iitbhu.ac.in (J. Prasad Chakraborty).

https://doi.org/10.1016/j.fuel.2019.116263
Received 31 May 2019; Received in revised form 8 August 2019; Accepted 21 September 2019
Available online 27 September 2019
0016-2361/

Nomenclature

Acronyms

HHV	Higher heating value (MJ/kg)
TGA	Thermogravimetric analysis
DTG	Differential thermogravimetry
T-220	Torrefied biomass obtained at 220 °C
T-250	Torrefied biomass obtained at 250 °C
T-280	Torrefied biomass obtained at 280 °C

Variables

k	Rate constant
α	fractional conversion
m_0	Initial mass of the sample (mg)
m_t	Mass of sample at any time t (mg)
m_f	Final mass of the sample (mg)
E_a	Activation energy (kJ/mol)
E_α	Activation energy at different conversion (kJ/mol)
A	Pre-exponential factor (s^{-1})
R	Universal gas constant
β	Heating rate (K/min)
T	Temperature (K)
T_α	Temperature at different conversion (K)
T_p	Peak temperature in the DTG curve (K)
ΔH	Change in enthalpy (kJ/mol)
ΔG	Change in Gibbs free energy (kJ/mol)
ΔS	Change in entropy (J/mol.K)
K_B	Boltzmann constant ($1.381*10^{-23}$ J/K)
h	Plank constant ($6.626*10^{-23}$ J.s),

models were dominant. Overall, results provide a deep understanding of kinetics and improved characteristics of torrefied biomass as good quality solid fuel.

1. Introduction

Depletion of fossil fuels and fast-growing population all around the world has an adverse impact on the energy supply chain which causes an increase in demand for energy in day to day life and it is predicted that energy requirement will be increased by 50% by the year 2050 [1]. Pollution and greenhouse gas effect caused by fossil fuels are also degrading the quality and creating an imbalance in the environment [2–4]. To overcome these defies researchers from all around the world started thinking about alternate source which provide renewable, clean and sustainable energy. Among various available renewable energy resources such as solar, wind [5], biomass, and hydrothermal; biomass has fascinated the most due to its large abundance, cheap and negligible market importance, easy accessibility, biodegradable, low greenhouse gas emission and carbon neutrality [6,7]. Also, biomass is the 4th largest source of energy after coal, petroleum and natural gas and it alone contributes 14–15% of world's energy supply and 38–43% of energy requirement in developing nations [8]. Various forms of biomass includes forest, agricultural and crop residue etc. [9]. Biomass comprises three major constituents: cellulose, hemicellulose, and lignin [4]. Each constituent comprises of approximately 40–60, 20–40 and 10–25 wt%, respectively, of total lignocellulosic biomass [10,11]. The thermal decomposition of these components takes place in different range of temperature. Generally, hemicellulose, cellulose, and lignin decompose in the temperature range of 220–315, 315–400, and 200–900 °C, respectively [4,10,12–14]. *Acacia nilotica*, (belongs to *Mimosaceae* family), a kind of forest tree, is mostly found in the Indian subcontinent, Africa, Australia, and South East Asian countries. It is a very good source of renewable biomass as it is fast growing and easy to spread by seeds. It is usually grown in leftover and unproductive land having poor growing condition. In the Indian perspective, *Acacia nilotica*, frequently known as Babool, usually grows in the northern part. In India, around six million tonnes of *Acacia nilotica* pod is generated every year [15,16]. These pods are commonly used to feed animals and as a fuel for heat generation in domestic purpose, textile mill and brick field due to its high calorific value and low smoke producing tendency. Thus, *Acacia nilotica* may be used for bio-energy generation.

The energy from biomass can be extracted through biological (enzymatic digestion and fermentation), and thermochemical (torrefaction, liquefaction, pyrolysis, gasification etc.) conversion routes; however later has gained dominance due to its fast and efficient nature [17]. Nonetheless, irrespective of many positives associated with biomass, the straightforward application of biomass during the thermochemical process cannot be proficient since it is associated with many inherent shortcomings like higher moisture content, lower higher heating value (HHV), higher O/C and H/C ratio and hygroscopic nature, which makes biomass inferior to coal [4,18,19]. Among the various explored processes, fortunately, torrefaction is a promising technique to upgrade physicochemical properties of biomass so that it can be used as a solid fuel in many processes like pyrolysis and gasification [20].

During torrefaction, biomass is heated in the inert environment at atmospheric pressure in the temperature range of 200–300 °C Preferred residence time is less than one hour along with a slow heating rate (<15 °C/min) [4,20–22]. The torrefied biomass exhibits improved characteristics than raw biomass in terms of less moisture content, higher HHV, lower H/C and O/C ratio. Torrefaction also improves the grindability and lowers the water sorption characteristics of biomass

Table 1
Proximate, ultimate, calorific value and fiber analysis of raw and torrefied biomass.

Analysis	Raw	T-220	T-250	T-280
Proximate analysis (wt %)				
Moisture content	6.46±0.42	3.46±0.37	1.47±0.08	0.85±0.10
Ash content	0.78±0.19	1.42±0.23	1.96±0.13	2.39±0.16
Volatile matter	79.08±1.80	61.48±1.27	46.45±1.18	40.15±1.17
Fixed carbon*	13.68±0.91	33.64±1.48	50.12±1.17	56.61±1.56
Ultimate analysis (wt%)				
Carbon	43.69±0.77	49.48±0.78	54.63±2.03	63.75±1.57
Hydrogen	7.54±0.77	6.77±0.25	3.83±0.22	2.62±0.36
Nitrogen	0.47±0.15	1.35±0.19	1.97±0.14	2.14±0.12
Oxygen*	48.30±0.73	42.40±1.11	39.57±1.00	31.49±0.61
H/C	0.17±0.06	0.13±0.03	0.07±0.01	0.04±0.008
O/C	1.10±0.12	0.85±0.11	0.72±0.07	0.49±0.12
Fiber analysis(wt %, dry basis)				
Hemicellulose	28.64±0.95	25.49±0.77	17.38±0.56	10.52±1.52
Cellulose	41.66±0.90	44.51±1.89	38.38±1.04	33.61±0.82
Lignin	24.20±0.43	27.71±1.49	41.25±1.24	54.24±1.41
Extractive*	5.50±0.48	2.29±0.23	2.99±0.24	1.63±0.26
Higher heating value (MJ/kg)	18.66±0.72	20.33±1.04	22.51±1.22	25.94±1.20
Solid yield (%)	–	71.28±1.85	57.09±1.20	42.71±1.48

*By difference

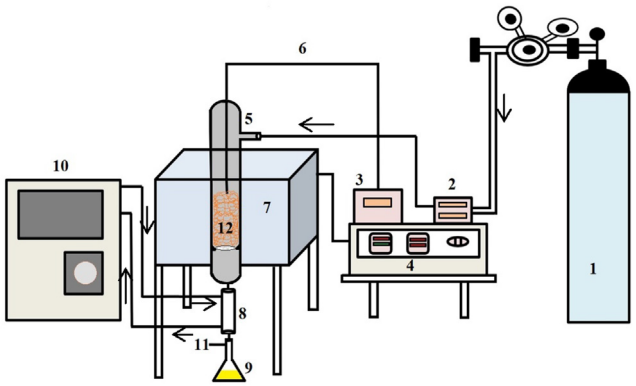

Fig. 1. Schematic diagram of experimental set-up: 1-nitrogen cylinder, 2-mass flow controller, 3-temperature measuring unit, 4- split tube furnace (NSW-104) controller, 5-long tube fixed bed reactor, 6-K-type thermocouple, 7- split tube furnace (NSW-104), 8-condenser, , 9-oil collector, 10- chiller (Eyela CA-1112CE), 11-gas collector, 12-biomass with ceramic wool bed.

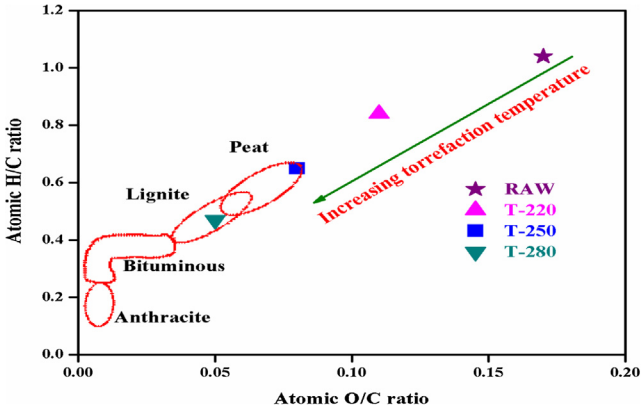

Fig. 2. van Krevelen diagram for raw and torrefied biomass.

[4,20–22]. Eventually, there are two ways through which energy can be extracted from the torrefied biomass viz. either direct use of treated biomass in pyrolysis and gasification or co-pyrolysis, co-gasification with other biomass, plastic and municipal waste. Besides, these days blending of torrefied biomass with coal in thermal power plants are common practice [23–28].

So, in order to explore the torrefied biomass and to achieve the best utilization for bio-energy generation, kinetic and thermodynamic parameters along with model prediction of reaction mechanism become essential. The recommendations suggested by the kinetic committee of the International Confederation for Thermal Analysis and Calorimetry (ICTAC), the thermogravimetric analysis (TGA) is one of the most prevalent and effective methods to describe the thermal decomposition behavior and kinetics of biomass and coal conversion [29]. Through TGA and DTG data, kinetic parameters such as activation energy and pre-exponential factor can be investigated. Furthermore, the thermodynamic parameters may also be interpreted based on the kinetic parameters.

In the past, a lot of work has been dedicated to investigating the kinetic and thermodynamic parameters of different biomass [12,30–37]. Conversely, stress over the torrefied biomass is relatively limited and thermodynamic parameters of torrefied biomass are barely reported. Bach et al. [21] examined the pyrolysis characteristics and kinetic study of torrefied biomass in different environment and reported that non-oxidative environment does not affect the kinetics of torrefied biomass pyrolysis. Ren at al. [4] investigated the torrefaction and pyrolysis of Douglas fir sawdust using TGA and concluded that pyrolysis of torrefied biomass obtained at higher temperature might be a multiple step reaction. Hu et al. [2] studied the thermal behavior and kinetics of pyrolysis of torrefied biomass pellets using three pseudo-component models. They observed that the contribution of hemicellulose decreases in reaction kinetics as activation energy decreases with an increase in torrefaction temperature. Asadieraghi et al. [38] investigated the pyrolysis kinetics of palm oil biomass using first-order reaction model. Doddapaneni et al. [33] investigated the influence of torrefaction on pyrolysis kinetics and reaction mechanism of eucalyptus clone. Arias et al. [39] investigated the effect of torrefaction on grindability and reactivity of woody biomass. They observed that torrefaction affected kinetic parameters in the first stage while parameters for the second stage remain unaffected. Bach et al. [22] preformed a comparative study on thermal degradation of Norway spruce wood through wet and dry torrefaction using independent parallel reaction model.

The kinetic parameters (activation energy, pre-exponential factor), thermodynamic parameters (enthalpy, Gibbs free energy, and entropy) and reaction mechanism are very important for design, optimization, and scaling of process reactor and parameters [2]. The behavior of

Table 2
Models of pyrolysis reaction with different values of $f(\alpha)$ and $g(\alpha)$.

Solid state process	Mechanism	$f(\alpha)$	$g(\alpha)$
One dimensional diffusion	D1	$1/(2\alpha)$	α^2
Two-dimensional diffusion (Valensi model)	D2	$[-\ln(1-\alpha)]^{-1}$	$(1-\alpha)\ln(1-\alpha)+\alpha$
Three-dimensional diffusion (Jander model model)	D3	$\frac{3}{2}(1-\alpha)^{2/3}[1-(1-\alpha)^{1/3}]^{-1}$	$[1-(1-\alpha)^{1/3}]^2$
Three-dimensional diffusion (Ginstlinge-Brounshtein model)	D4	$\frac{3}{2}[(1-\alpha)^{1/3}-1]^{-1}$	$1-\frac{2}{3}\alpha-(1-\alpha)^{2/3}$
Contracting cylinder	F2	$2(1-\alpha)^{1/3}$	$1-(1-\alpha)^{1/2}$
Contracting sphere	F3	$(1-\alpha)^{2/3}$	$1-(1-\alpha)^{1/3}$
Power law	P2/3	$\frac{2}{3}\alpha^{-1/2}$	$\alpha^{3/2}$
Power law	P2	$2\alpha^{1/2}$	$\alpha^{1/2}$
Power law	P3	$3\alpha^{2/3}$	$\alpha^{1/3}$
Power law	P4	$4\alpha^{3/4}$	$\alpha^{1/4}$
Avrami-Erofeev	A1	$\frac{1}{2}(1-\alpha)[-\ln(1-\alpha)]^{1/3}$	$[-\ln(1-\alpha)]^{2/3}$
Avrami-Erofeev	A2	$2(1-\alpha)[-\ln(1-\alpha)]^{1/2}$	$[-\ln(1-\alpha)]^{1/2}$
Avrami-Erofeev	A3	$3(1-\alpha)[-\ln(1-\alpha)]^{2/3}$	$[-\ln(1-\alpha)]^{1/3}$
Avrami-Erofeev	A4	$4(1-\alpha)[-\ln(1-\alpha)]^{3/4}$	$[-\ln(1-\alpha)]^{1/4}$
1st order random nucleation having one nucleus on individual particle	R1	$(1-\alpha)$	$-\ln(1-\alpha)$
2nd order random nucleation having two nucleus on individual particle	R2	$(1-\alpha)^2$	$(1-\alpha)^{-1}-1$
3rd order random nucleation having three nucleus on individual particle	R3	$(1-\alpha)^3$	$\frac{1}{2}[(1-\alpha)^{-2}-1]$

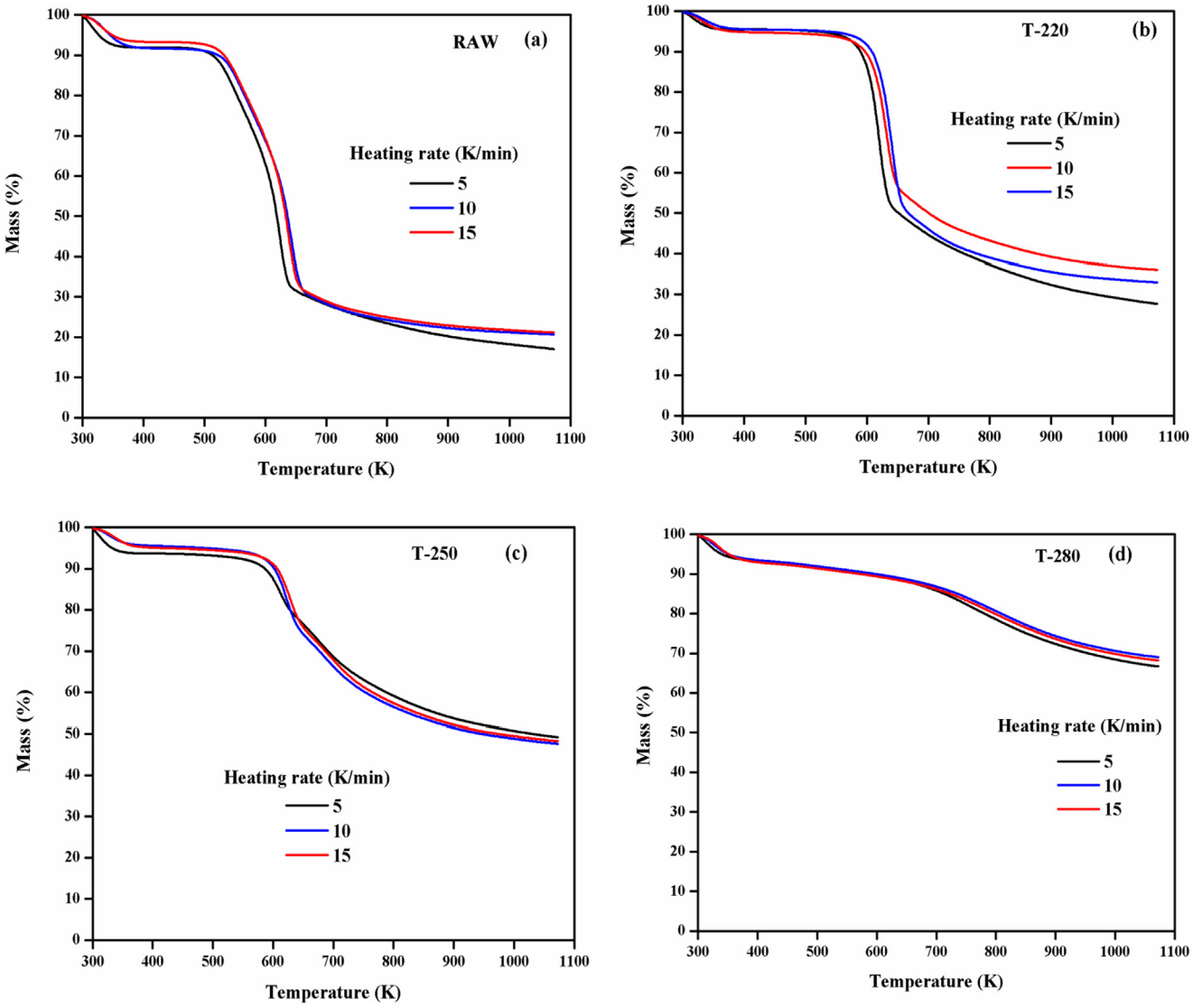

Fig. 3. TGA analysis of raw and torrefied biomass at different heating rate: (a) Raw, (b) T-220 (c) T-250, and (d) T-280.

torrefied biomass towards thermochemical conversion might be different from raw biomass. Also, during blending of torrefied biomass with coal in thermal power plant, the process will be affected by the distinctive kinetic, thermodynamic parameters and reaction mechanism followed individually by torrefied biomass and coal. So, the deep insight about the kinetic, thermodynamic parameter as well as reaction mechanism of torrefied biomass is required. However, to the best of our knowledge, the thermodynamic parameters of torrefied biomass have not been reported; however, kinetic parameters and reaction mechanism during pyrolysis of torrefied biomass has been scarcely reported.

For that reason, in present study torrefaction of *Acacia nilotica* was carried out in a lab scale fixed-bed reactor. The physicochemical characteristics of raw and torrefied biomass were derived from proximate, ultimate, HHV and fiber analysis. Then pyrolysis of torrefied biomass was performed using TGA. Based on the TGA data, kinetic (activation energy and pre-exponential factor) and thermodynamic (enthalpy, Gibbs free energy, and entropy) parameters of raw and torrefied biomass were obtained. Four different isoconversional models viz. KAS, OWF, Friedman, and Starink were employed to calculate the kinetic parameters. Thermodynamic parameters were calculated based on the kinetic parameters obtained from the KAS method. In addition, reaction mechanism was proposed for pyrolysis of raw and torrefied biomass.

2. Materials and methods

2.1. Material collection, preparation, and characterization

A*cacia nilotica* was collected from the rural area nearby Indian Institute of Technology (Banaras Hindu University) Varanasi. Biomass sample was sun-dried to remove surface moisture. Then, cutting mill (Retsch model SM 300, Germany) was used to reduce the particle size followed by screening to get fine particles between 0.5 and 0.6 mm. The sun-dried sample was further dried overnight in a hot air oven maintained at 70 °C and kept in a desiccator for further use. Proximate analysis, moisture content (MC), ash content (AC) and volatile matter (VM) of raw and torrefied samples were performed according to standard methods ASTM E871, ASTM E1755, and ASTM E872, respectively. Fixed carbon (FC) was calculated by difference. The CHNS analysis of raw and torrefied biomass was performed by using the CHNS analyzer (EURO EA3000, EURO VECTOR instrument and software, ITALY). Oxygen content was calculated by difference assuming negligible sulfur content. Bomb calorimeter (IKA, C-200 model, Germany) is used to estimate the HHV of raw and torrefied biomass. The hemicellulose, cellulose, and lignin components of biomass were determined following

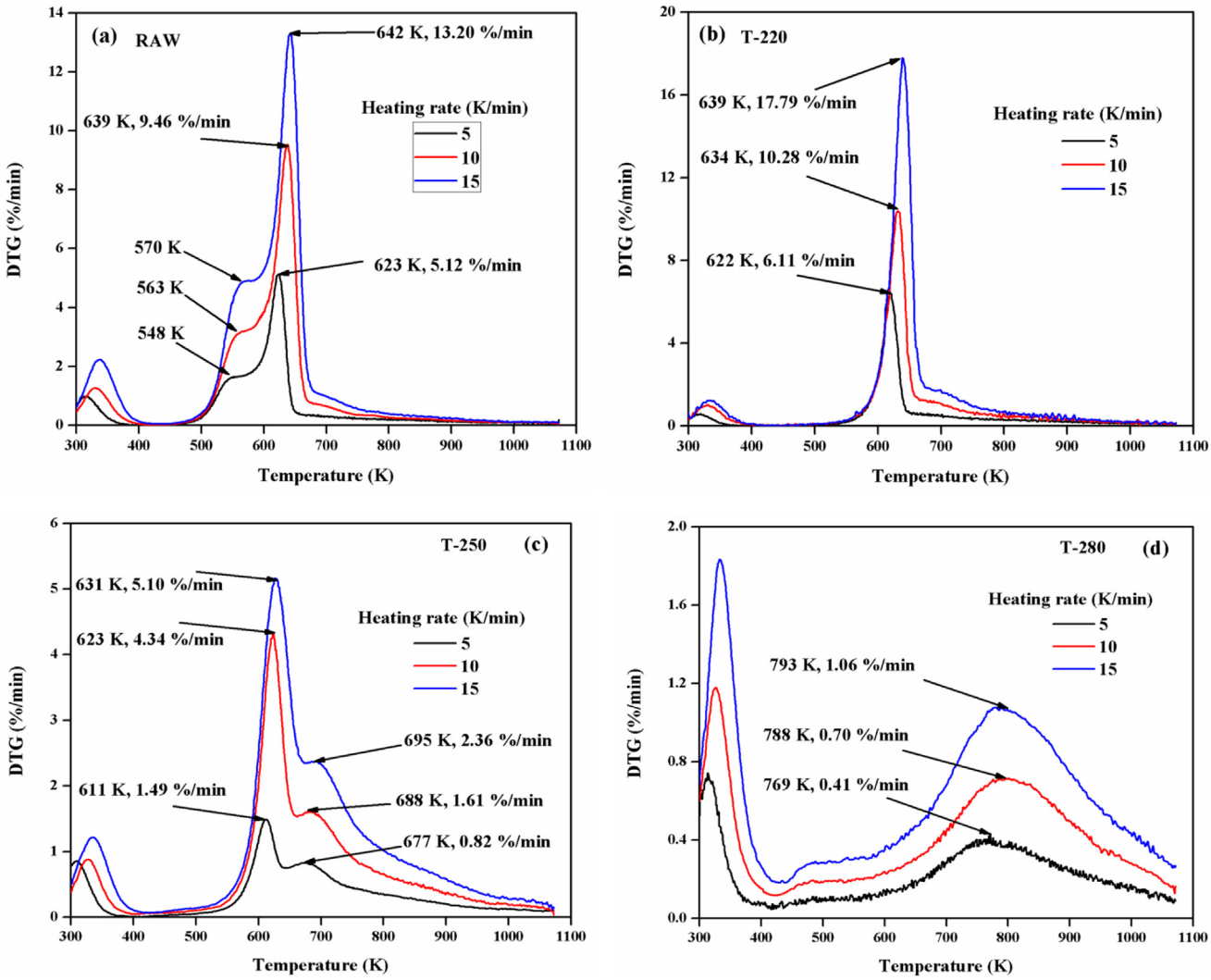

Fig. 4. DTG analysis of raw and torrefied biomass at different heating rate: (a) Raw, (b) T-220 (c) T-250, and (d) T-280.

the protocol mentioned by Bledzki et al. [40]. Extractive component was calculated by difference. The proximate, ultimate, HHV and other parameters are presented in Table 1 and the relevant discussion is carried out in subsequent sections. In the present study, dried *Acacia nilotica* is labeled as RAW and torrefied *Acacia nilotica* is labeled as T-X, where X indicates torrefaction temperature. For example, T-250 indicates torrefied *Acacia nilotica* which was obtained by torrefaction at 250 °C.

2.2. Experimental procedure for torrefaction and pyrolysis of torrefied biomass

The torrefaction of biomass was carried out in a laboratory fixed bed reactor at 220, 250, and 280 °C with a residence time of 40 min, and a heating rate of 15 °C/min. The schematic diagram of the experimental setup is shown in Fig. 1. Mass flow controller (Bronkhorst, Netherlands) was used to purge the reactor by nitrogen gas (99.99% purity) at a flow rate of 40 mL/min for 45 min to remove any residual oxygen from the reactor. In each set of experiment, 10 g of biomass sample was kept on support of ceramic wool inside the reactor. The temperature inside the reactor was measured by using a K-type thermocouple. The solid residue (torrefied biomass) was taken out from the reactor when it got cooled to room temperature, and then it was weighed. Each experiment was repeated twice, and the average value has been reported. The thermogravimetric analyzer (NETZSCH TG 209F1 Libra) was used to carry out pyrolysis of raw and torrefied biomass at three different heating rates 5, 10, 15 K/min, between the temperature ranges from 298 to 1073 K. Nitrogen gas (99.99%, purity), at a flow rate of 20 mL/min was used as a carrier. 5 mg of each biomass sample was taken. In each experiment, initially, nitrogen gas was purged into the TGA for 20 min at an initial temperature to avoid undesirable oxidation of sample during pyrolysis. The sample was kept for 20 min at 1073 K when the experiment was over. The uncertainty in the experimental measurement of the parameters has been given in the Supplementary Material section (S1).

2.3. Kinetic study

The chemical composition and physical characteristics vary from one biomass to another. Consequently, pyrolysis becomes a complex process and various biomass shows different behavior [30,35]. The TGA and DTG data were used to obtain the kinetic and thermodynamic parameters for thermal degradation of raw and torrefied biomass during pyrolysis. The general pyrolysis reaction can be represented as [12,31]:

$$\text{Biomass} \xrightarrow{k} \text{Bio} - \text{char} + \text{volatile}$$

A general expression for non-isothermal kinetics for solid decomposition can be expressed as follows:

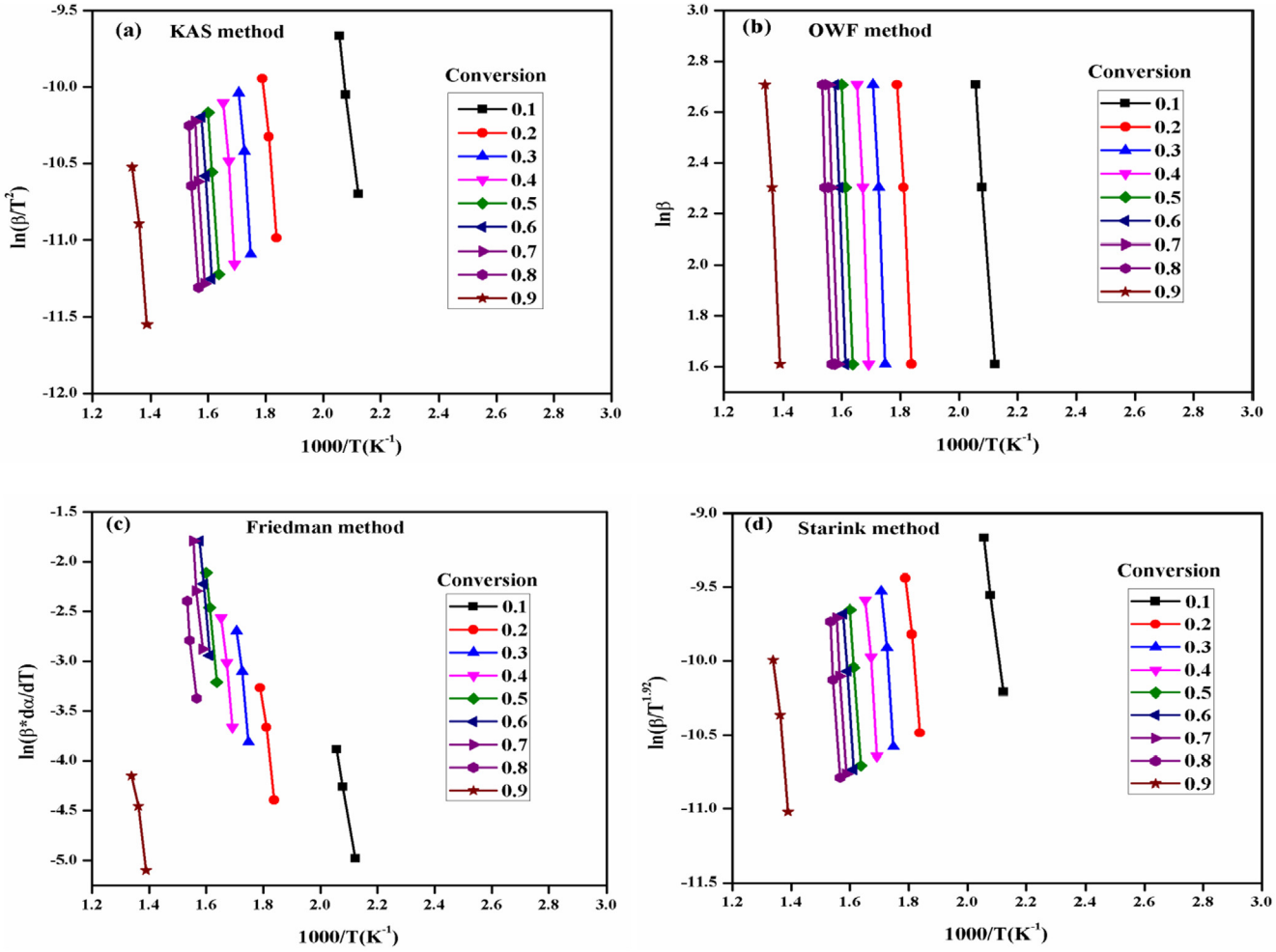

Fig. 5. Kinetic plot for raw biomass using (a) KAS, (b) OWF, (c) Friedman, and (d) Starink models.

$$\frac{d\alpha}{dt} = k(T)f(\alpha) \tag{1}$$

where, k is the rate constant, and α is the fractional conversion during thermal decomposition of solid biomass. Biomass conversion can be defined as follows:

$$\alpha = \frac{m_0 - m_t}{m_0 - m_f} \tag{2}$$

where, m_0 is the initial mass of the sample, m_t is the mass of sample at any time t, and m_f is the final mass of the sample.

The rate constant is a function of temperature and may be expressed as follows:

$$k(T) = Ae^{-E_a/RT} \tag{3}$$

where E_a is activation energy, A is pre-exponential factor and R is universal gas constant.

Combining Eqs. (1) and (3) gives the fundamental expression (4) for the analytical method to calculate kinetic parameters, on the basis of TGA data.

$$\frac{d\alpha}{dt} = Ae^{-E_a/RT}f(\alpha) \tag{4}$$

The TGA analysis was carried out at a constant heating rate given as:

$$\beta = \frac{dT}{dt} \tag{5}$$

The conversion can be expressed as the function of temperature. However, the temperature is dependent on the heating rate also. Therefore,

$$\frac{d\alpha}{dT} = \frac{d\alpha}{dt}\frac{dt}{dT} \tag{6}$$

$$\frac{d\alpha}{dT} = \frac{d\alpha}{dt}\frac{1}{\beta} \tag{7}$$

Combining Eqs. (4) and (7)

$$\frac{d\alpha}{dT} = \frac{A}{\beta}e^{-E_a/RT}f(\alpha) \tag{8}$$

Integrating both sides of Eqs. (8) gives:

$$g(\alpha) = \int_0^\alpha \frac{d\alpha}{f(\alpha)} = \frac{A}{\beta}\int_0^T e^{-E_a/RT}dT \tag{9}$$

where, $g(\alpha)$ is the integral function of conversion α. The kinetic model $f(\alpha)$ is an algebraic expression related with a physical model which describes the kinetics of the solid state reaction. Functional forms of $f(\alpha)$ and $g(\alpha)$ representing different reaction mechanism are listed in Table 2. These expressions can be used to predict the reaction mechanism, reflected by the dynamic TGA curves. In the present study, the activation energy was obtained from non-isothermal TGA. The methods used to determine the kinetic parameters are isoconversional or model free methods. The kinetic parameters were estimated from numerous plots at different heating rates at same level of conversion.

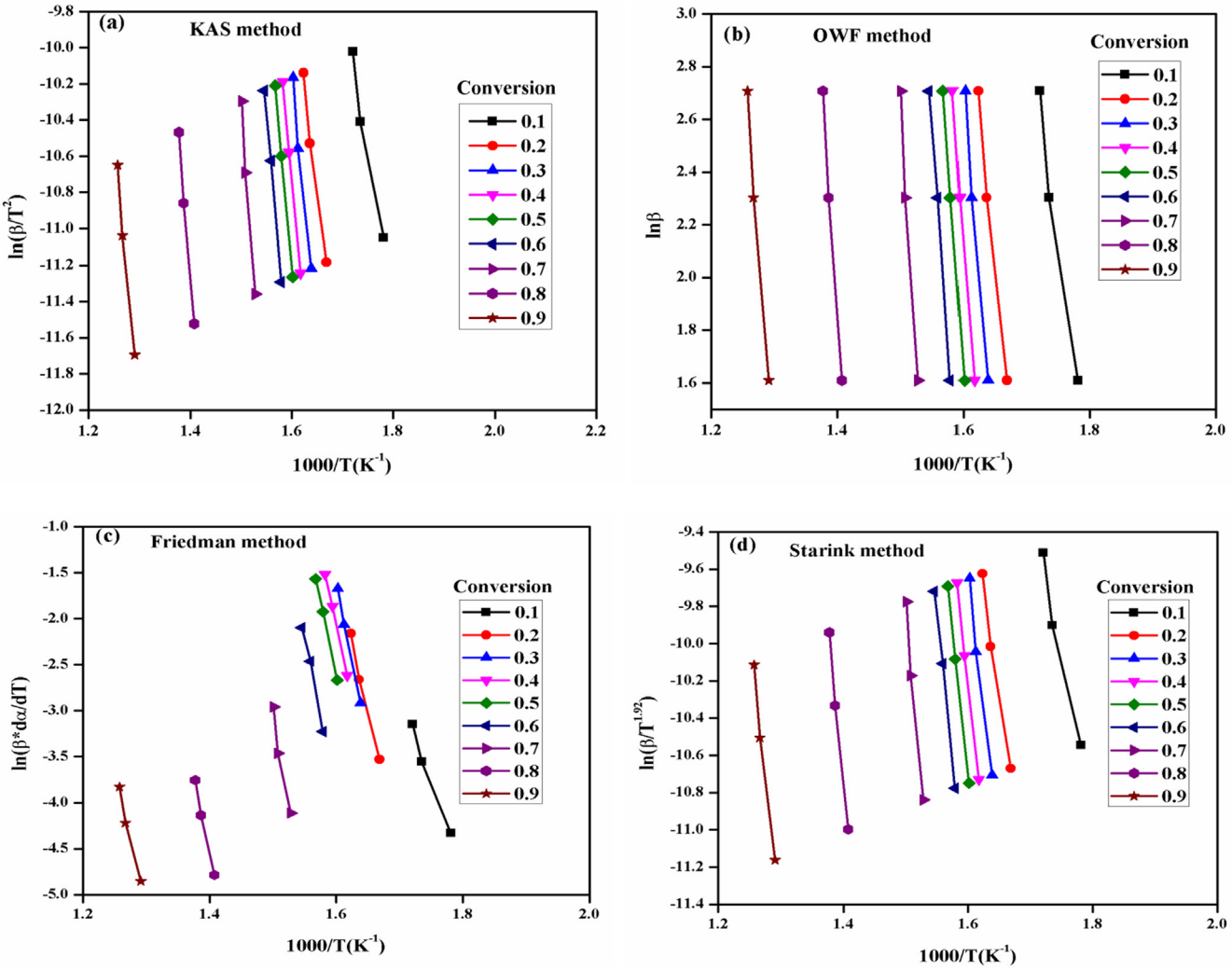

Fig. 6. Kinetic plot for T-220 using (a) KAS, (b) OWF, (c) Friedman, and (d) Starink models.

2.4. Model-free isoconversional methods

The thermal decomposition of biomass is very complex process and it is characterized by multiple reactions with different rates. Thus, simple kinetic model cannot be applicable for such reactions. To investigate the in-depth analysis of thermal decomposition of biomass, isoconversional models are frequently used. The isoconversional models used in present work are: (1) Kissinger-Akahira-Sunose (KAS) method, (2) Ozawa-Wall- Flynn (OWF) method, (3) Friedman method, and (4) Starink method. The models, their descriptions and formulations have been provided as Supplementary Material (S2).

2.5. Prediction of reaction model

The model for solid state reaction during pyrolysis of biomass is investigated by Z-master plot associated with Criado method (Eqs. (10)) [41]. Master plots are the plots which depend on the reaction kinetic model however they are independent of kinetic parameters like activation energy and pre-exponential factor [42].

$$\frac{Z(\alpha)}{Z(0.5)} = \frac{f(\alpha)\times g(\alpha)}{f(0.5)\times g(0.5)} = \left(\frac{T_\alpha}{T_{0.5}}\right)^2 \times \frac{(d\alpha/dT)_\alpha}{(d\alpha/dT)_{0.5}} \quad (10)$$

The above Equation is employed to generate the master plots equivalent to various solid-state reaction mechanism as mentioned in Table 2. In this Equation, the term $[f(\alpha)\times g(\alpha)/f(0.5)\times g(0.5)]$ will give a theoretical curve, which signifies the characteristics of each reaction mechanism. While, the term $[(T_\alpha/T_{0.5})^2 \times ((d\alpha/dT)_\alpha/(d\alpha/dT)_{0.5})]$ will reduce to a curve obtained from experimental values. The conversion value $\alpha = 0.5$ is selected as a reference value, at which, master plot from all the reaction mechanism and experimental curve will intersect to each other at the value of $[Z(\alpha)/Z(0.5)] = 1$. The principal reaction mechanism for experimental value is decided by comparing the theoretical and experimental curves. The theoretical curve which is closest to the experimental curve is selected as reaction mechanism [42–44].

2.6. Estimation of pre-exponential factor and thermodynamic parameter

Using isoconversional methods discussed earlier in section 2.5, activation energy was calculated at different level of conversion; however, the pre-exponential factor and reaction mechanism given by isoconversional method is not reliable [42]. For pre-exponential factor Kissinger's method was used given by Eqs. (11). Kissinger's method is employed at different heating rate; however it gives only a single value of activation energy for overall conversion process. Thus it was not used to calculate activation energy in this study. Once, the activation energy is known at different value of conversion, Eqs. (12) can be used to calculate pre-exponential factor. In this study, activation energy obtained from KAS method was used to calculate pre-exponential factor.

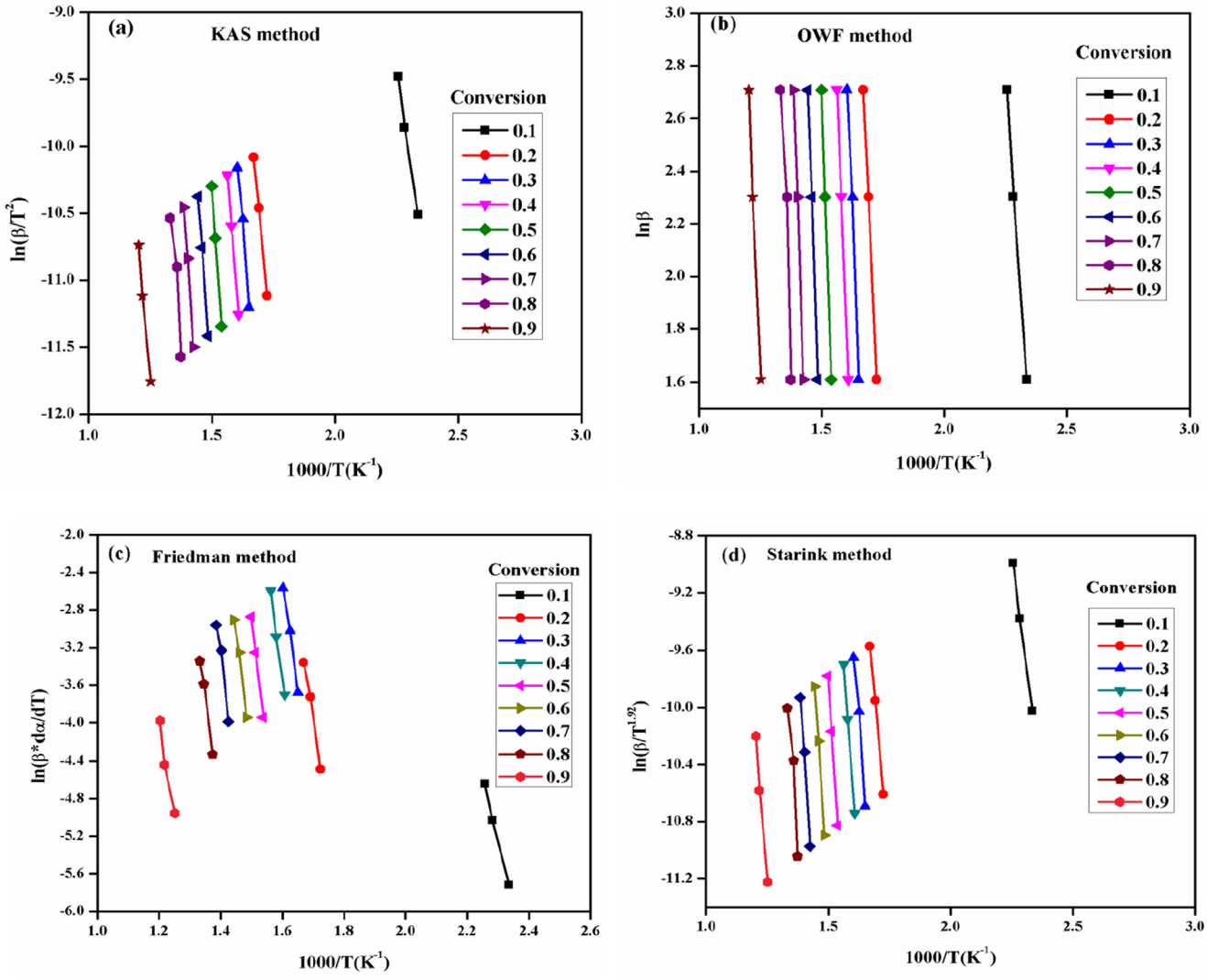

Fig. 7. Kinetic plot for T-250 using (a) KAS, (b) OWF, (c) Friedman, and (d) Starink models.

$$\ln\left(\frac{\beta}{T_p^2}\right) = \ln\left(\frac{AR}{E}\right) - \frac{E}{RT_p} \tag{11}$$

$$A = \beta.\ E_\alpha.\ \mathrm{Exp}\left(\frac{E_\alpha}{RT_p}\right)/(\mathrm{R}.\ T_p 2) \tag{12}$$

Once the activation energy and pre-exponential factor was known at different level of conversion, the thermodynamic parameters such as change in enthalpy (ΔH), change in Gibbs free energy (ΔG), and change in entropy (ΔS) were calculated using the equation (13)-(15).

$$\Delta H = E_\alpha - RT_\alpha \tag{13}$$

$$\Delta G = E_\alpha + \mathrm{R}.\ T_p.\ \ln\left(\frac{K_B.\ T_m}{h.\ A}\right) \tag{14}$$

$$\Delta S = \frac{\Delta H - \Delta G}{T_p} \tag{15}$$

where, K_B is the Boltzmann constant ($1.381*10^{-23}$ J/K), h is the Plank constant ($6.626*10^{-23}$ J.s), and T_p, is the peak temperature in the DTG curve.

3. Results and discussion

3.1. Yield of product and physicochemical characteristics of raw and torrefied biomass

Table 1 represents the yield of solid product at 220, 250, and 280 °C with a constant residence time of 40 min and a heating rate of 15 °C/min. The major mass loss during torrefaction occurs due to loss of water along with the loss of lighter volatile matter through devolatilization process [45,46]. At lower temperature, the decomposition of hemicellulose, cellulose, and lignin is not significant, which results in higher solid yield. However, at a higher temperature, considerable amount of hemicellulose degraded with simultaneous decomposition of cellulose and lignin. Hence, the solid yield also decreases notably. In addition, the decomposition of hydroxyl group intensified at a higher temperature resulting in release of more volatiles. Furthermore, the composition of biomass (hemicellulose, cellulose, and lignin), also governs the quality and yield of products from torrefaction. Biomass having higher hemicellulose content yields less solid product than liquid and gas during torrefaction since the decomposition of hemicellulose takes place at relatively lower temperature [45,47].

The proximate, ultimate, HHV and fiber analysis of raw and torrefied biomass (T-220, T-250, and T-280) are presented in Table 1. It was observed that moisture content and volatile matter of raw biomass

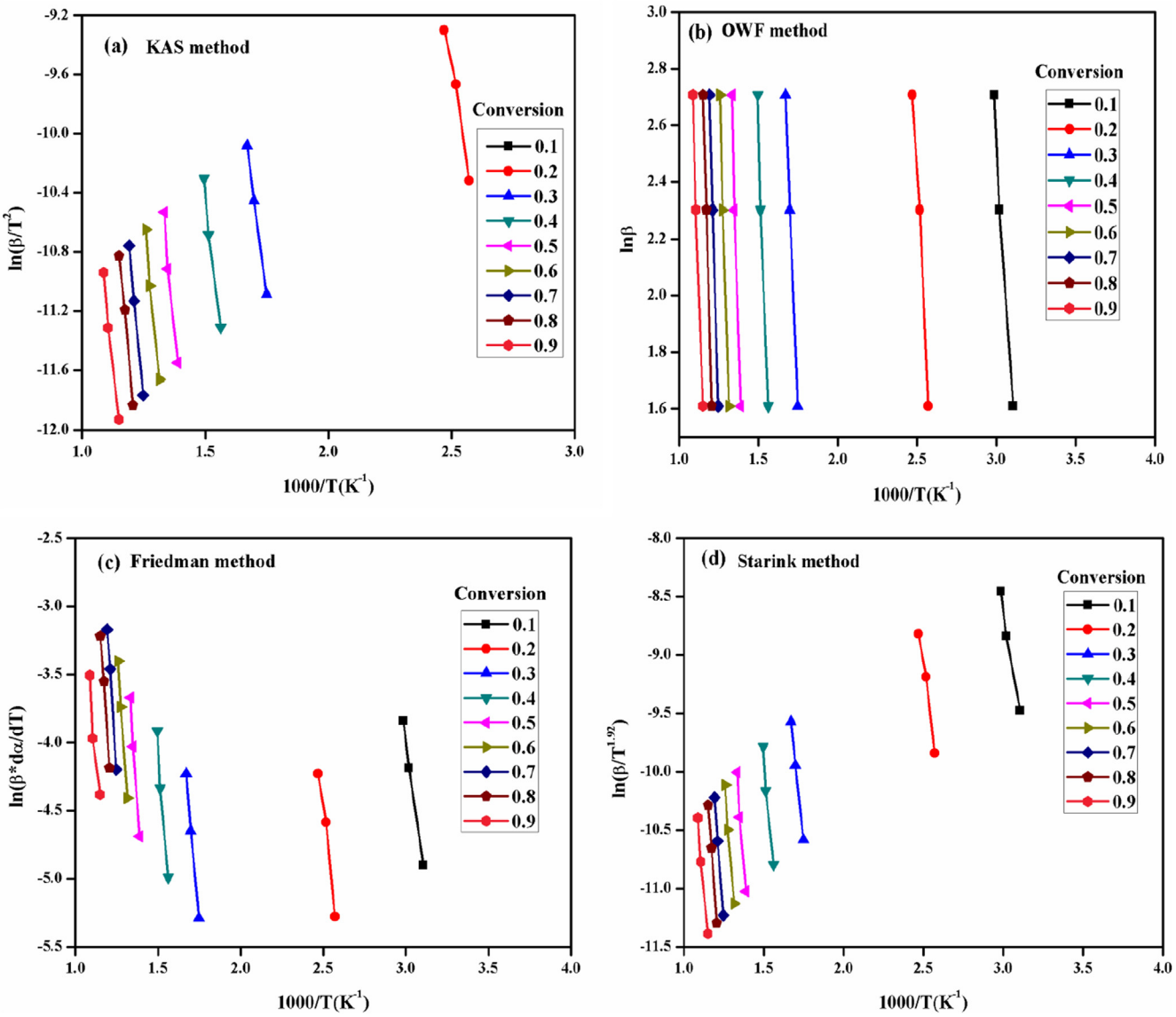

Fig. 8. Kinetic plot for T-280 using (a) KAS, (b) OWF, (c) Friedman, and (d) Starink models.

decreased from 6.5 to 0.88% and 79.85 to 38.52%, respectively, when the temperature of torrefaction increased from 220 to 280 °C. On the other hand, fixed carbon and ash content increased from 13.02 to 58.42%, and 0.55 to 2.18%, respectively, under similar temperature conditions. Thus, it can be seen that temperature has pronounced effect on moisture content, volatile matter, fixed carbon, and ash content. It should be noted that the ash content of torrefied biomass was much lower than that of coal (~13.71 wt%) [48]. Thus, the increase in operating cost associated with coal application like ash deposition and disposal can be minimized by consuming torrefied biomass in preference to coal. Increase in fixed carbon content of torrefied biomass was due to more devolatilization at enhanced temperature, thereby causing removal of water and light volatile matter [49]. Frequently, van Krevelen diagram (Fig. 2) is used to understand the consequence of ultimate analysis on biomass and coal [46]. It was noticed that H/C and O/C ratio of raw biomass decreased from 0.17 to 0.04 and from 1.09 to 0.49, respectively, when temperature of torrefaction increased from 220 to 280 °C (Table 1). The removal of hydrogen and oxygen during torrefaction is more pronounced than release of carbon. Accordingly, both H/C and O/C ratio decreased significantly. In addition, the comparative upsurge in the carbon content and fixed carbon through torrefaction is accountable for higher HHV of torrefied biomass than the raw biomass. The HHV of raw biomass increased from 18.89 MJ/kg to 25.87 MJ/kg, when temperature increased from 220 to 280 °C; which was an increase of 26.98%. Generally, the HHV of coal is found to be in the range of 25–35 MJ/kg [46]. Thus, torrefied biomass may be compared with lignite coal, and during co-combustion, it can be mixed with coal in thermal power plants for generation of energy.

Table 1 also represents the fiber analysis of raw and torrefied biomass. The hemicellulose, cellulose, lignin, and extractives present in raw biomass are 28.51, 41.66, 23.90, and 5.95%, respectively. The hemicellulose and extractives content decreased while the lignin content increased with increasing temperature during torrefaction. On the other hand, the cellulose content increased at lower temperature (T-220) and then goes on decreasing on further increase in temperature. Hemicellulose, cellulose, and extractives decreased by 69.34, 21.84, and 53.61%, respectively. Though, lignin content increased by 57.27%. Hence, it was noted that, in the course of torrefaction, the decomposition of hemicellulose is more pronounced than the decomposition of cellulose and lignin.

3.2. Thermogravimetric analysis

The pyrolysis behavior of raw and torrefied biomass (T-220, T-250,

Table 3
The activation energy of raw and torrefied biomass at different level of conversion using KAS, OWF, Friedman and Starink methods.

Conversion	KAS method		OWF method		Friedman method		Starink method	
	E (kJ/mol)	R^2	E (kJ/mol)	R^2	E (kJ/mol)	R^2	E (kJ/mol)	R^2
RAW								
0.1	128.89	0.9966	136.84	0.9970	137.67	0.9993	129.21	0.9966
0.2	175.68	0.9900	184.84	0.9910	189.74	0.9873	176.04	0.9901
0.3	207.89	0.9806	217.52	0.9823	220.22	0.9810	208.29	0.9807
0.4	222.09	0.9804	232.03	0.9832	231.85	0.9926	222.49	0.9809
0.5	235.78	0.9992	246.05	0.9992	248.57	0.9992	236.20	0.9992
0.6	245.41	0.9970	255.83	0.9972	267.41	0.9981	245.82	0.9970
0.7	266.40	0.9929	276.98	0.9934	267.21	0.9656	266.82	0.9929
0.8	251.46	0.9882	262.18	0.9891	230.97	0.9792	251.88	0.9882
0.9	169.81	0.9853	182.01	0.9873	157.45	0.9729	170.30	09,854
Average	**211.49**		**221.58**		**216.78**		**211.89**	
T-220								
0.1	135.29	0.9760	144.77	0.9789	157.20	0.9865	135.66	0.9761
0.2	186.95	0.9893	197.05	0.9904	245.77	0.9910	187.35	0.9894
0.3	236.64	0.9873	246.90	0.9883	284.35	0.9979	237.04	0.9874
0.4	248.88	0.9991	259.28	0.9920	262.14	0.9990	249.30	0.9991
0.5	253.79	0.9991	264.27	0.9992	266.64	0.9996	252.20	0.9991
0.6	264.06	0.9969	274.70	0.9971	283.84	0.9892	264.48	0.9969
0.7	314.44	0.9768	325.41	0.9783	334.18	0.9497	314.88	0.9769
0.8	282.87	0.9935	294.80	0.9940	276.53	0.9941	283.34	0.9936
0.9	251.34	0.9878	264.37	0.9889	245.85	0.9856	251.85	0.9878
Average	**241.58**		**252.39**		**261.83**		**241.78**	
T-250								
0.1	106.37	0.9973	113.61	0.9976	111.15	0.9985	106.66	0.9973
0.2	157.23	0.9975	167.03	0.9976	172.55	0.9904	157.62	0.9973
0.3	180.94	0.9783	191.17	0.9806	193.80	0.9918	181.35	0.9998
0.4	190.84	0.9998	201.33	0.9998	201.57	0.9949	191.26	0.9998
0.5	219.65	0.9930	230.60	0.9993	225.79	0.9999	220.09	0.9993
0.6	213.20	0.9972	224.56	0.9975	213.46	0.9919	213.66	0.9972
0.7	219.84	0.9923	231.76	0.9931	218.15	0.9596	220.32	0.9924
0.8	205.14	0.9915	217.12	0.9869	197.77	0.9899	205.32	0.9853
0.9	172.38	0.9939	185.91	0.9947	161.16	0.9636	172.92	0.9940
Average	**185.06**		**198.89**		**188.37**		**185.46**	
T-280								
0.1	68.42	0.9874	73.87	0.9891	72.00	0.9968	68.64	0.9874
0.2	83.81	0.9846	90.41	0.9868	86.54	0.9784	84.07	0.9847
0.3	105.77	0.9993	115.49	0.9994	110.80	0.9966	106.16	0.9993
0.4	119.48	0.9818	130.33	0.9846	126.83	0.9779	119.91	0.9819
0.5	146.14	0.9797	158.34	0.9824	147.71	0.9869	146.62	0.9796
0.6	145.44	0.9875	158.35	0.9893	146.17	0.9958	145.96	0.9876
0.7	147.74	0.9994	161.38	0.9995	153.28	0.9947	148.29	0.9994
0.8	151.78	0.9941	165.89	0.9951	146.64	0.9904	152.34	0.9942
0.9	127.93	0.9886	142.78	0.9907	108.73	0.9243	128.52	0.9887
Average	**121.83**		**132.98**		**122.07**		**122.27**	

and T-280) at a heating rate of 5, 10, and 15 K/min is shown in Figs. 3a-d and 4a-d. The whole degradation process can be categorized into three major stages: (1) drying, (2) devolatilization, and (3) char formation. The first stage is accompanied with the elimination of surface moisture and some light volatile compounds [50], and it was noticed that mass loss owing to moisture for torrefied biomass (T-220, T-250, and T-280) is slightly lesser than the raw biomass. The second stage is associated with the devolatilization process which was accompanied by major mass loss from biomass due to degradation of the major portion of hemicellulose and cellulose. At, the third stage, lignin decomposition is more pronounced. The TGA curve in this zone has a flat and long tail. Accordingly, the mass loss in this stage is lower than the second stage. Considering a fixed amount of mass loss for example 10%, for raw and torrefied biomass (T-220, T-250, and T-280), at a heating rate of 5 K/min, it was attained at 520, 572, 586, and 610 K, respectively. It shows that decomposition shifted to a higher temperature in case of torrefied biomass and extent of the shift in temperature increases with increase in temperature during torrefaction. The decomposition of hemicellulose and cellulose takes place between 200 and 350 °C, whereas; lignin decomposes in a wider range of temperature between 280 and 600 °C [4,7]. It was noticed from Table 1 that major fraction of hemicellulose degraded along with limited degradation of cellulose during torrefaction. This may be the reason for shifting of onset devolatilization temperature in case of torrefied biomass. Additionally, inconsistency in thermal degradation of biomass component is also responsible for deviation in residual char yield. The residual char yield after pyrolysis of raw and torrefied biomass (T-220, T-250, and T-280) at a heating rate of 5 K/min, was observed to be 17.09, 27.76, 49.30, and 66.72%, respectively. In addition, slight variation in residual char yield was also observed due to the variation of heating rate. The higher residual char yield in case of torrefied biomass may be due to large mass loss through decomposition of hemicellulose and lignin and also due to the cross-linkage reaction during the pyrolysis of torrefied biomass [4,51,52]. Thus, it may be mentioned that higher the torrefaction temperature, higher will be the char yield during pyrolysis.

Fig. 4a-d is present the DTG curve of raw and torrefied biomass. In DTG curve, the presence of shoulder on the left side of the plot describes the degradation of hemicellulose in the biomass and is typically noted at around 573 K [7,53]. In case of raw biomass, similar shoulders appear at 548, 563, and 573 K at a heating rate of 5, 10, and 15 K/min, respectively, as shown in Fig. 4a. On the other hand, the similar shoulder disappeared in case of torrefied biomass (T-220, T-250, and T-280) (Fig. 4b-d), suggesting that major fraction of hemicellulose has already being degraded in the course of torrefaction. Yang et al. [7]

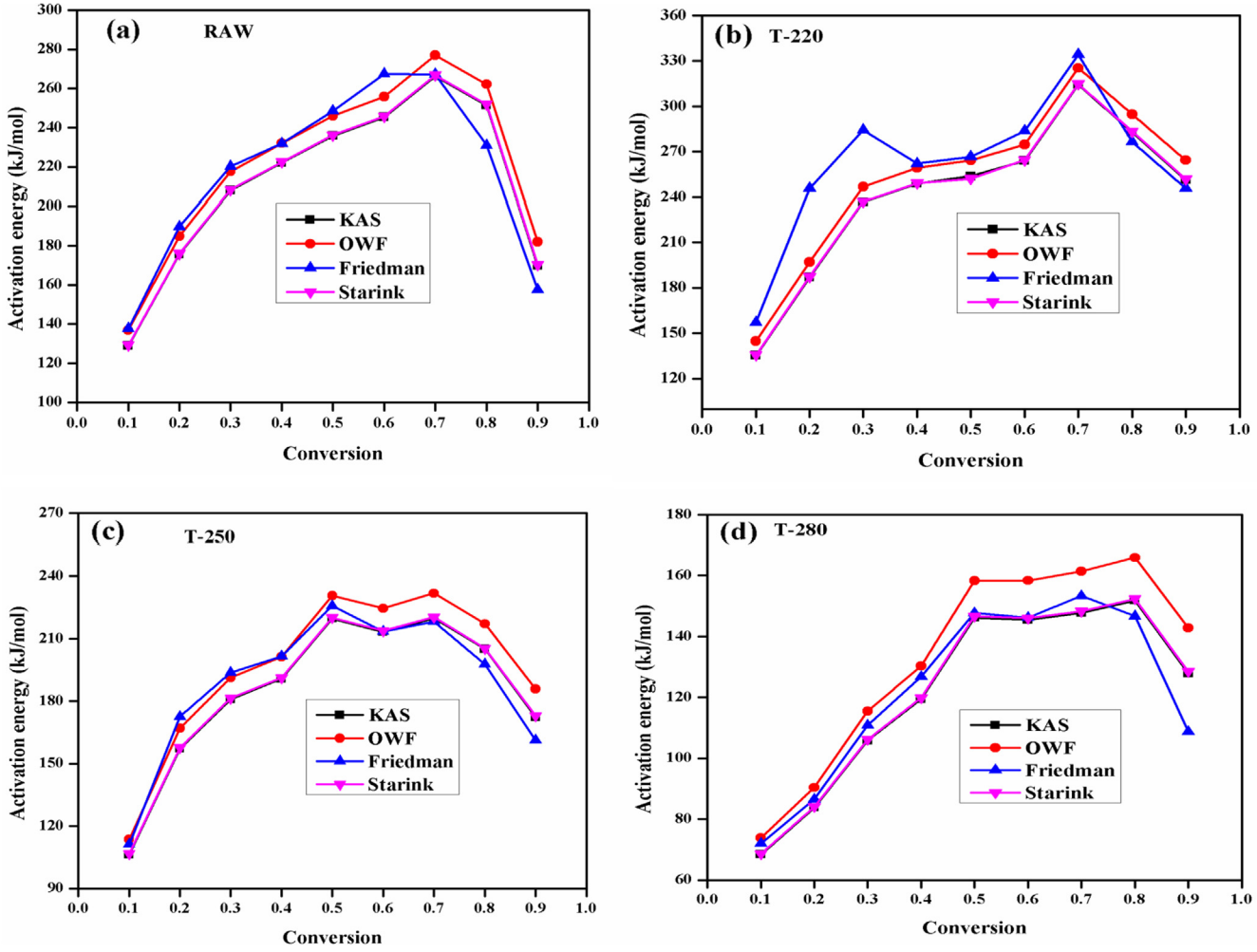

Fig. 9. Variation of activation energy with conversion using different models: (a) Raw, (b) T-220 (c) T-250, and (d) T-280.

reported that peaks appeared in the DTG curve with maximum weight loss signifies the occurrence of cellulose in the biomass. The temperature noted at the peaks in DTG curve for raw biomass was 623, 639, and 642 K at a heating rate of 5, 10, and 15 K/min, respectively, as shown in Fig. 4a. For torrefied biomass (T-220) the cellulose peak temperature was noted at 622, 634, and 639 K, at a heating rate of 5, 10, and 15 K/min, respectively (Fig. 4b). However, in case of torrefied biomass (T-250), peak temperature was noted at 611, 623, and 623 K, at a heating rate of 5, 10, and 15 K/min, respectively. In addition, another peak to the right side of the cellulose peak can be observed at 677, 688, and 695 K, at a heating rate of 5, 10, and 15 K/min, respectively (Fig. 4c). The appearance of second peak may be attributed to the degradation of lignin. Conversely, in case of torrefied biomass (T-280), in place of hemicellulose and cellulose peak, a broader peak at 769, 783, and 798 K, at a heating rate of 5, 10, and 15 K/min, respectively, were observed (Fig. 4d). These broader peaks are associated with the degradation of lignin. Similar results were also observed by Tong et al. [54] Furthermore, comparing the peak intensity of raw and torrefied biomass (T-220, T-250, and T-280) at particular heating rate say 5 K/min, it was found to be 5.12, 6.11, 1.49 and 0.41 wt%/min, respectively. The increase in peak intensity of T-220 (Fig. 4b) than the raw biomass may be due to higher amount of relative cellulose content in T-220 than the raw biomass as presented in Table 1. On further increase in temperature, there was decrease in peak intensity.

3.3. Kinetic analysis

The estimation of the kinetic parameters is very useful for efficient design and scaling of process reactors at industrial level [31]. The decomposition kinetic analysis of raw and torrefied biomass was performed by applying four isoconversional methods such as KAS, OWF, Friedman and Starink at different degree of conversion ranging from 0.1 to 0.9. The isoconversional plots obtained from four methods for raw and torrefied biomass (T-220, T-250, and T-280) are shown in Figs. 5–8. It can be seen that, with an increase in conversion, the slope of isoconversional lines are also changing. The slopes of these lines are used to obtain the activation energy. Thus, the value of activation energy also changes accordingly as presented in Table 3. The variation of activation energy with the degree of conversion is shown in Fig. 9. The activation energy obtained from KAS, Friedman, and Starink methods for raw and torrefied biomass (T-220, T-250, and T-280) are comparable. However, slightly higher activation energy was noticed in case of OWF method as depicted by Table 3. The difference in activation energy from different method may be due to the assumptions and approximation adopted by different methods [31]. For example, in case of OWF method, for integral term $\int_0^T \exp\left(\frac{-E}{RT}\right)dT$, the analytical solution is not possible. Thus, Doyle's approximation was used, though Friedman method does not adopt any such approximation [37,55]. The value of activation energy changes with conversion during the pyrolysis, illustrating the multi-stage kinetics rather than single stage and complexity of process during biomass conversion through pyrolysis. Therefore, the overall decomposition of biomass is established by a multi-stage

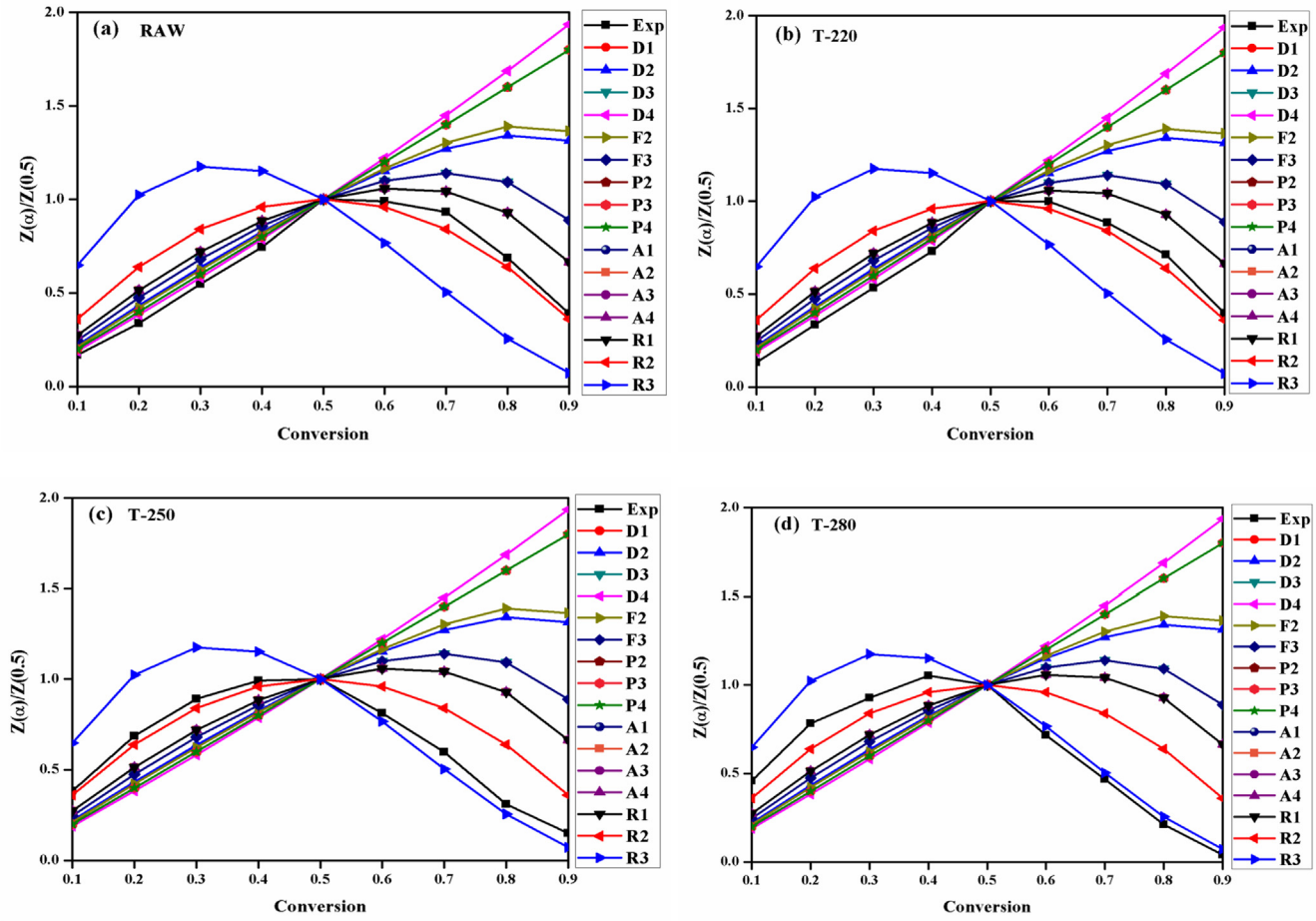

Fig. 10. Theoretical and experimental plots for prediction of solid state reaction mechanism using Criado method (Z-master plot): (a) Raw, (b) T-220 (c) T-250, and (d) T-280.

reaction mechanism where every single stage added partially to global mechanism depending upon the extent of decomposition.

The activation energy is the minimum amount of energy required to proceed a reaction. Thus, higher activation energy hinders the start of a reaction. Activation energy is also useful in deciding the reactivity of fuel [31]. The activation energy of raw and torrefied biomass (T-220, T-250, and T-280) was calculated using KAS, OWF, Friedman and Starink methods represented by Eqs. (9), 10, 13, and 15, respectively as discussed in section 2.5. For raw biomass, the calculated value of activation energy from these methods varied within 211.49–221.58 kJ/mol. The activation energy for decomposition of torrefied biomass (T-220, T-250, and T-280) varied within 241.58–261.83, 185.06–198.89, and 121.83–132.98 kJ/mol, respectively. The activation energy of component of biomass (hemicellulose, cellulose and, and lignin) are different. Vamvuka et al. [56] reported the activation energy of cellulose, hemicellulose, and lignin in the range of 145–285, 90–125 and 30–39 kJ/mol individually. The highest activation energy was reported for cellulose, followed by hemicellulose and then lignin. Thus the biomass having higher amount of cellulose will have higher activation energy. The relative amount of cellulose in T-220 is higher than the raw biomass as presented in Table 1. Accordingly, higher activation energy in case of T-220 than the raw biomass was noticed. On further increasing the temperature during torrefaction, the degradation of cellulose also becomes significant. Thus activation energy of T-250 and T-280 are lower than raw biomass. The lower activation energy of T-280 makes it suitable for thermochemical conversion. In addition, it can be used in co-firing with other biomass or coal etc.

3.4. Prediction of reaction mechanism (Criado analysis)

Criado analysis was employed to investigate the reaction mechanism during pyrolysis of raw and torrefied biomass (T-220, T-250, and T-280) at a different level of conversion at a heating rate of 10 K/min. The standard kinetic models selected are mentioned in Table 2. The master plots for raw and torrefied biomass are shown in Fig. 10a-d at conversion from 0.1 to 0.9.

3.4.1. Reaction mechanism at lower conversion (α< 0.5)

Table 4 represents the decomposition mechanism followed by raw and torrefied biomass (T-220, T-250, and T-280). For raw and torrefied biomass (T-220) at conversion less than 0.5, the closest match with the theoretical curve is associated with D1, D2, D3 and D4 mechanism which corresponds to one dimensional diffusion model, two-dimensional diffusion (Valensi model), three-dimensional diffusion (Jander model) and three-dimensional diffusion (Ginstlinge-Brounshtein model), respectively. Whereas, torrefied biomass T-250 follows the R2 model which corresponds to 2nd order random nucleation having two nucleus on individual particle (R2) and torrefied biomass T-280, followed the R2 and R3 model, which corresponds to 2nd order random nucleation having two nucleus on individual particle and 3rd order random nucleation having three nucleus on individual particle (R3), respectively, for the conversion less than 0.5. In case of raw and torrefied biomass (T-220), the dominance of diffusion model may be due to higher volatile content as presented in Table 1. However, in case of torrefied biomass (T-250 and T-280), the volatile matter is already released in the course of torrefaction. Accordingly, random nucleation

Table 4
Predicted models for raw and torrefied biomass.

Biomass	Solid state process	
	Conversion < 0.5	Conversion > 0.5
Raw	Diffusion models (D1, D2, D3 and D4) D1 $f(\alpha) = 2(1-\alpha)[-\ln(1-\alpha)]^{1/2}$ $g(\alpha) = [-\ln(1-\alpha)]^{1/2}$ D2 $f(\alpha) = [-\ln(1-\alpha)]^{-1}$ $g(\alpha) = (1-\alpha)\ln(1-\alpha)+\alpha$ D3 $f(\alpha) = \frac{3}{2}(1-\alpha)^{2/3}[1-(1-\alpha)^{1/3}]^{-1}$ $g(\alpha) = [1-(1-\alpha)^{1/3}]^2$ D4 $f(\alpha) = \frac{3}{2}[(1-\alpha)^{1/3}-1]^{-1}$ $g(\alpha) = 1-\frac{2}{3}\alpha-(1-\alpha)^{2/3}$	2nd order random nucleation having two nucleus on individual particle (R2) R2 $f(\alpha) = (1-\alpha)^2$ $g(\alpha) = (1-\alpha)^{-1}-1$ Avrami-Erofeev models (A1, A2, A3 and A4) A1 $f(\alpha) = \frac{1}{2}(1-\alpha)[-\ln(1-\alpha)]^{1/3}$ $g(\alpha) = [-\ln(1-\alpha)]^{2/3}$ A2 $f(\alpha) = 2(1-\alpha)[-\ln(1-\alpha)]^{1/2}$ $g(\alpha) = [-\ln(1-\alpha)]^{1/2}$ A3 $f(\alpha) = 3(1-\alpha)[-\ln(1-\alpha)]^{2/3}$ $g(\alpha) = [-\ln(1-\alpha)]^{1/3}$ A4 $f(\alpha) = 4(1-\alpha)[-\ln(1-\alpha)]^{3/4}$ $g(\alpha) = [-\ln(1-\alpha)]^{1/4}$
T-220	Diffusion models (D1, D2, D3 and D4) D1 $f(\alpha) = 2(1-\alpha)[-\ln(1-\alpha)]^{1/2}$ $g(\alpha) = [-\ln(1-\alpha)]^{1/2}$ D2 $f(\alpha) = [-\ln(1-\alpha)]^{-1}$ $g(\alpha) = (1-\alpha)\ln(1-\alpha)+\alpha$ D3 $f(\alpha) = \frac{3}{2}(1-\alpha)^{2/3}[1-(1-\alpha)^{1/3}]^{-1}$ $g(\alpha) = [1-(1-\alpha)^{1/3}]^2$ D4 $f(\alpha) = \frac{3}{2}[(1-\alpha)^{1/3}-1]^{-1}$ $g(\alpha) = 1-\frac{2}{3}\alpha-(1-\alpha)^{2/3}$	2nd order random nucleation having two nucleus on individual particle (R2) R2 $f(\alpha) = (1-\alpha)^2$ $g(\alpha) = (1-\alpha)^{-1}-1$
T-250	2nd order random nucleation having two nucleus on individual particle (R2) $f(\alpha) = (1-\alpha)^2$ $g(\alpha) = (1-\alpha)^{-1}-1$	3rd order random nucleation having three nucleus on individual particle (R3) $f(\alpha) = (1-\alpha)^3$ $g(\alpha) = \frac{1}{2}[(1-\alpha)^{-2}-1]$
T-280	2nd order random nucleation having two nucleus on individual particle (R2) R2 $f(\alpha) = (1-\alpha)^2$ $g(\alpha) = (1-\alpha)^{-1}-1$ 3rd order random nucleation having three nucleus on individual particle (R3) R3 $f(\alpha) = (1-\alpha)^3$ $g(\alpha) = \frac{1}{2}[(1-\alpha)^{-2}-1]$	3rd order random nucleation having three nucleus on individual particle (R3) $f(\alpha) = (1-\alpha)^3$ $g(\alpha) = \frac{1}{2}[(1-\alpha)^{-2}-1]$

models become prominent. These results are in good agreement with the published results obtained by Doddapaneni et al. [33], Mishra et al. [43], Poletto et al. [44], and Vlaev et al. [57]. Diffusion models are associated with the diffusion of gaseous products from the reactant samples. As the conversion increases, the thickness of the product layer around the sample increases. This layer around the sample can hinder the transfer of heat from the external source. Accordingly, the decomposition of the sample will be affected. Therefore, diffusion becomes the rate-determining step during the pyrolysis process at low conversion.

3.4.2. Reaction mechanism at higher conversion (α> 0.5)

For higher degree of conversion (from 0.5 to 0.9), the reaction mechanism was followed by raw and torrefied biomass are presented in Table 4. For raw biomass (T-220) at conversion greater than 0.5, the closest match with the theoretical curve is associated with R2, which corresponds to 2nd order random nucleation having two nuclei on individual particle and Avrami-Erofeev models (A1, A2, A3, and A4) which is associated with nucleation and growth. Whereas, torrefied biomass T-220 follows the R2 model which corresponds to 2nd order random nucleation having two nuclei on individual particle (R2) and torrefied biomass T-250 and T-280 both followed R3 model, which corresponds to 3rd order random nucleation having three nuclei on individual particle (R3). During the decomposition process, higher conversion was achieved at relatively higher temperature. At higher temperature, cleavage of some ordered cellulose may take place which gets converted into chain of lower molecular mass. This chain of lower molecular mass might act as a site for random nucleation growth and degradation reaction.

3.5. Thermodynamic parameters

The thermodynamic parameters were calculated by using Eqs. (18)–(21) based on apparent activation energy obtained from the KAS method at a heating rate of 10 K/min and corresponding values are presented in Table 5. Furthermore, the low value of heating rate was selected to avoid the effect of interaction between the constituents, which shows the pronounced effect at a higher heating rate [37]. The values of pre-exponential factor for raw and torrefied biomass (T-220, T-250, and T-280) at different conversion, obtained using KAS method at a heating rate of 10 K/min ranges from 10^{10} to 10^{18}, 10^{10} to 10^{25}, 10^{8} to 10^{18} and 10^{3} to 10^{9}, respectively. Pre-exponential factor depicts the nature of the complex associated with the reaction. The low value of pre-exponential factor signifies the closed complex whereas high value signifies the simple complex [31,37]. Turmanova et al. [58] investigated that the value of empirical pre-exponential factor for first-order reaction generally varies from 10^{4} to 10^{18} s^{-1}. The variation in pre-exponential factor may be due to the complex nature of biomass and also due to complex thermal degradation of biomass. It was also noted that the value of pre-exponential factor is in line with the value of activation energy. At particular conversion, higher pre-exponential factor was noted at higher value of activation energy.

The Enthalpy is a thermodynamic property which signifies the total heat content of a system. In case of biomass pyrolysis, it represents the total amount of heat taken by the biomass for its conversion into different products like bio-char, bio-oil, and gases [59]. The change in enthalpy with different level of conversion calculated from KAS method at 10 K/min is given in Table 5. The enthalpy for raw and torrefied biomass (T-220, T-250, and T-280) varies from 124.97 to 261.18, 130.60–309.04, 102.72–214.14, and 65.66–144.69 kJ/mol,

Table 5
Thermodynamic parameters for pyrolysis of raw and torrefied biomass at a heating rate of 10 K/min.

Conversion	A (s^{-1})	ΔH (kJ/mol)	ΔG (kJ/mol)	ΔS (J/mol.K)
RAW				
0.1	1.42×10^{10}	124.97	164.33	−62.13
0.2	1.33×10^{11}	171.18	199.54	−44.96
0.3	6.88×10^{13}	203.17	199.36	5.45
0.4	1.07×10^{15}	217.22	199.33	27.52
0.5	1.51×10^{16}	230.73	199.32	48.72
0.6	9.69×10^{16}	243.22	199.32	63.71
0.7	5.53×10^{18}	261.20	199.35	96.42
0.8	3.11×10^{17}	246.18	199.32	72.93
0.9	4.23×10^{10}	163.83	199.59	−56.56
T-220				
0.1	5.61×10^{10}	130.60	163.47	−51.82
0.2	1.39×10^{15}	181.97	162.93	30.01
0.3	2.18×10^{19}	231.59	162.78	108.48
0.4	2.33×10^{20}	243.77	162.79	127.67
0.5	6.04×10^{20}	248.63	162.79	135.33
0.6	4.40×10^{21}	258.84	162.81	151.39
0.7	7.39×10^{25}	309.04	163.00	230.24
0.8	1.67×10^{23}	277.00	162.86	179.95
0.9	3.76×10^{20}	244.91	162.78	129.48
T-250				
0.1	2.62×10^{8}	102.72	162.48	−95.73
0.2	6.99×10^{12}	152.31	160.45	−13.03
0.3	7.76×10^{14}	175.82	159.72	25.79
0.4	5.51×10^{15}	185.57	159.44	41.86
0.5	1.64×10^{18}	214.15	158.71	88.81
0.6	4.58×10^{17}	207.50	158.87	77.91
0.7	1.70×10^{18}	213.91	158.71	88.43
0.8	9.32×10^{16}	198.98	159.07	63.94
0.9	1.42×10^{14}	165.55	159.97	8.93
T-280				
0.1	3.70×10^{3}	65.66	216.51	−2.20
0.2	4.57×10^{4}	80.50	215.16	−1.60
0.3	1.56×10^{6}	100.87	213.61	−1.06
0.4	1.38×10^{7}	113.98	212.80	−0.82
0.5	9.21×10^{8}	139.96	211.45	−0.48
0.6	8.26×10^{8}	138.91	211.49	−0.49
0.7	1.18×10^{9}	140.87	211.38	−0.47
0.8	2.23×10^{9}	144.69	211.20	−0.43
0.9	5.24×10^{7}	120.40	212.34	−0.71

respectively. It was noticed that at each level of conversion, the difference of energy between the activation energy and enthalpy for raw and torrefied biomass (T-220, T-250, and T-280) was ~2–6, ~5–6, ~4–7, and ~3–7 kJ/mol. This difference is attributed to the difference between activated complex formed during the decomposition and initial, raw and torrefied biomass. Mehmood et al. [60] illustrated that difference of activation energy and enthalpy suggested that product formation can be achieved by providing 2–6, 5–6, 4–7, and 3–7 kJ/mol of energy in case of raw and torrefied biomass, respectively. Vlaev et al. and Loy et al. [61,62] illustrated that lower difference between the activation energy and enthalpy favors the formation of an activated complex which finally leads to bioenergy production through pyrolysis.

Gibbs free energy (ΔG) indicates the total increase in energy of a system for the formation of the activated complex [31,58]. The change in ΔG at each conversion value calculated using KAS method at 10 K/min is given in Table 5. The ΔG for raw and torrefied biomass (T-220, T-250, and T-280) varies from 164.33 to 199.59, 162.78–163.47, 158.71–162.48, and 211.20–216.51 kJ/mol, respectively. It can confer that, for raw biomass, the variation in ΔG is higher; however, for torrefied biomass the value of ΔG, remains almost constant for all value of conversion from 0.1 to 0.9. A positive value of ΔG for raw and torrefied biomass (T-220, T-250, and T-280) reveals the unfavorable reactions that consume a considerable amount of energy to occur [32]. Similar results of ΔG for different biomass have been reported by Xu et al. [63] for rice straw, Ahmad et al. [64] for para grass, and Huang et al. [34] for sewage sludge.

The entropy, being a state function, represents the degree of disorder or randomness associated with the reaction system. The change in entropy (ΔS) at different value of conversion is given in Table 5. It was found that ΔS for raw and torrefied biomass (T-220 and T-250) has both positive and negative values varies in the range of −44.96 to 96.42, −51.82 to 230.24, and −13.03 to 88.81 J/mol.K, respectively. The larger value of ΔS indicates that biomass sample is away from the thermodynamic equilibrium, while smaller value of ΔS means that biomass sample is acquiring a new state which is approaching it to state of thermodynamic equilibrium. However, T-280 has only negative ΔS in the range of −2.20 to −0.43 J/mol.K. The negative value of entropy is the result of disordered nature of product formed through bond dissociation. The low value of entropy also suggests that material has just passed through some physical and chemical changes, which bring the material to the state of thermodynamic equilibrium during the pyrolysis process [31,37].

4. Conclusions

Torrefaction of *Acacia nilotica* was performed in a fixed-bed reactor at three different temperatures 220, 250 and 280 °C, keeping residence time and heating rate constant. The physicochemical characteristics of raw and torrefied biomass (T-220, T-250 and T-280) were compared. The TGA of raw and torrefied biomass was performed at three different heating rate viz. 5, 10 and 15 K/min. Based on the result of TGA, kinetic, thermodynamic parameters and reaction mechanism during pyrolysis of raw and torrefied biomass were investigated. Physicochemical analysis revealed that torrefied biomass has much improved properties than raw biomass in term of lower moisture and volatile matter, higher fixed carbon content and HHV than the raw biomass. Compositional analysis showed that at lower temperature during torrefaction, the relative cellulose content in the torrefied biomass (T-220) is higher than the raw biomass, while, it goes on decreasing on further increase in temperature. The higher cellulose content attributed to higher activation energy of T-220 than raw biomass. The average activation energy of torrefied biomass obtained at 280 °C (T-280) is 42.39% lower than the raw biomass. A minor difference between activation energy and enthalpy favors the formation of activated complex. Accordingly, bio-energy generation through pyrolysis can be positively attained. It is noticed that at lower conversion value ($\alpha \leq 0.5$) the diffusion mechanism was rate determining for raw and T-220, however, for T-250 and T-280, the 2nd order random nucleation model is dominant for rate determination. At higher conversion ($\alpha \geq 0.5$), raw and T-220 follow the 2nd order random nucleation and Avrami-Erofeev models, while, in case of T-250 and T-280, 3rd order random nucleation is dominant.

Finally, it may be concluded that the behavior of raw and torrefied biomass towards thermochemical is quite different. The torrefied biomass has much improved properties than the raw biomass which makes it good quality solid fuel for bio-energy generation. Also, it can be blended with coal in thermal power plants.

Acknowledgement

The authors acknowledge the funding from the Science and Engineering Research Board (SERB), Government of India, New Delhi, India, through fund no. SR/FTP/ETA-56/2012.

Appendix A. Supplementary data

Supplementary data to this article can be found online at https://doi.org/10.1016/j.fuel.2019.116263.

References

[1] Anahas AMP, Muralitharan G. Characterization of heterocystous cyanobacterial

strains for biodiesel production based on fatty acid content analysis and hydrocarbon production. Energy Convers Manag 2018;157:423–37.
[2] Hu Q, Yang H, Xu H, Wu Z, Lim CJ, Bi XT. Thermal behavior and reaction kinetics analysis of pyrolysis and subsequent in-situ gasification of torrefied biomass pellets. Energy Convers Manag 2018;161:205–14.
[3] Kambo HS, Dutta A. Comparative evaluation of torrefaction and hydrothermal carbonization of lignocellulosic biomass for the production of solid biofuel. Energy Convers Manag 2015;105:746–55.
[4] Ren S, Lei H, Wang L, Bu Q, Chen S, Wu J. Thermal behaviour and kinetic study for woody biomass torrefaction and torrefied biomass pyrolysis by TGA. Biosyst Eng 2013;116(4):420–6.
[5] Gonçalves da Silva C. Renewable energies: Choosing the best options. Energy 2010;35(8):3179–93.
[6] Raheem A, Wan Azlina WAKG, Taufiq Yap YH, Danquah MK, Harun R. Thermochemical conversion of microalgal biomass for biofuel production. Renew Sustain Energy Rev 2015;49:990–9.
[7] Yang H, Yan R, Chen H, Lee DH, Zheng C. Characteristics of hemicellulose, cellulose and lignin pyrolysis. Fuel 2007;86(12):1781–8.
[8] Ertaş M, Hakkı Alma M. Pyrolysis of laurel (Laurus nobilis L.) extraction residues in a fixed-bed reactor: characterization of bio-oil and bio-char. J Anal Appl Pyrolysis 2010;88(1):22–9.
[9] Mohan D, Pittman CU, Steele PH. Pyrolysis of Wood/Biomass for Bio-oil: A Critical Review. Energy Fuels 2006;20(3):848–89.
[10] Granados DA, Chejne F, Basu P. A two dimensional model for torrefaction of large biomass particles. J Anal Appl Pyrolysis 2016;120:1–14.
[11] Parthasarathy P, Narayanan KS, Arockiam L. Study on kinetic parameters of different biomass samples using thermo-gravimetric analysis. Biomass Bioenergy 2013;58:58–66.
[12] Slopiecka K, Bartocci P, Fantozzi F. Thermogravimetric analysis and kinetic study of poplar wood pyrolysis. Appl Energy 2012;97:491–7.
[13] van der Stelt MJC, Gerhauser H, Kiel JHA, Ptasinski KJ. Biomass upgrading by torrefaction for the production of biofuels: A review. Biomass Bioenergy 2011;35(9):3748–62.
[14] Bach Q-V, Skreiberg Ø. Upgrading biomass fuels via wet torrefaction: A review and comparison with dry torrefaction. Renew Sustain Energy Rev 2016;54:665–77.
[15] Barman K, Rai SN. In vitro Nutrient Digestibility, Gas Production and Tannin Metabolites of Acacia nilotica Pods in Goats. Asian-Australas J Anim Sci 2008;21(1):59–65.
[16] Garg R, Anand N, Kumar D. Pyrolysis of babool seeds (Acacia nilotica) in a fixed bed reactor and bio-oil characterization. Renew Energy 2016;96:167–71.
[17] Dacres OD, Tong S, Li X, Zhu X, Edreis EMA, Liu H. Pyrolysis kinetics of biomasses pretreated by gas-pressurized torrefaction. Energy Convers Manag 2019;182:117–25.
[18] Winzer F, Kraska T, Elsenberger C, Kötter T, Pude R. Biomass from fruit trees for combined energy and food production. Biomass Bioenergy 2017;107:279–86.
[19] Liu Y, Guo F, Li X, Li T, Peng K, Guo C. Catalytic Effect of Iron and Nickel on Gas Formation from Fast Biomass Pyrolysis in a Microfluidized Bed Reactor: A Kinetic Study. Energy Fuels 2017;31(11):12278–87.
[20] Chen Y-C, Chen W-H, Lin B-J, Chang J-S, Ong HC. Impact of torrefaction on the composition, structure and reactivity of a microalga residue. Appl Energy 2016;181:110–9.
[21] Bach Q-V, Trinh TN, Tran K-Q, Thi NBD. Pyrolysis characteristics and kinetics of biomass torrefied in various atmospheres. Energy Convers Manag 2017;141:72–8.
[22] Bach Q-V, Tran K-Q, Skreiberg Ø. Comparative study on the thermal degradation of dry- and wet-torrefied woods. Appl Energy 2017;185:1051–8.
[23] Pan YG, Velo E, Roca X, Manyà JJ, Puigjaner L. Fluidized-bed co-gasification of residual biomass/poor coal blends for fuel gas production. Fuel 2000;79(11):1317–26.
[24] Bada SO, Falcon RMS, Falcon LM. Investigation of combustion and co-combustion characteristics of raw and thermal treated bamboo with thermal gravimetric analysis. Thermochim Acta 2014;589:207–14.
[25] Vuthaluru HB. Thermal behaviour of coal/biomass blends during co-pyrolysis. Fuel Process Technol 2004;85(2):141–55.
[26] Kastanaki E, Vamvuka D, Grammelis P, Kakaras E. Thermogravimetric studies of the behavior of lignite–biomass blends during devolatilization. Fuel Process Technol 2002;77–78:159–66.
[27] Zhang L, Xu S, Zhao W, Liu S. Co-pyrolysis of biomass and coal in a free fall reactor. Fuel 2007;86(3):353–9.
[28] Moghtaderi B, Meesri C, Wall TF. Pyrolytic characteristics of blended coal and woody biomass. Fuel 2004;83(6):745–50.
[29] Vyazovkin S, Burnham AK, Criado JM, Pérez-Maqueda LA, Popescu C, Sbirrazzuoli N. ICTAC Kinetics Committee recommendations for performing kinetic computations on thermal analysis data. Thermochim Acta 2011;520(1):1–19.
[30] Sriram A, Swaminathan G. Pyrolysis of Musa balbisiana flower petal using thermogravimetric studies. Bioresour Technol 2018;265:236–46.
[31] Kaur R, Gera P, Jha MK, Bhaskar T. Pyrolysis kinetics and thermodynamic parameters of castor (Ricinus communis) residue using thermogravimetric analysis. Bioresour Technol 2018;250:422–8.
[32] Mallick D, Poddar MK, Mahanta P, Moholkar VS. Discernment of synergism in pyrolysis of biomass blends using thermogravimetric analysis. Bioresour Technol 2018;261:294–305.
[33] Doddapaneni TRKC, Konttinen J, Hukka TI, Moilanen A. Influence of torrefaction pretreatment on the pyrolysis of Eucalyptus clone: A study on kinetics, reaction mechanism and heat flow. Ind Crops Prod 2016;92:244–54.
[34] Huang J, Liu J, Chen J, Xie W, Kuo J, Lu X. Combustion behaviors of spent mushroom substrate using TG-MS and TG-FTIR: Thermal conversion, kinetic, thermodynamic and emission analysis. Bioresour Technol 2018;266:389–97.
[35] Huang X, Cao J-P, Zhao X-Y, Wang J-X, Fan X, Zhao Y-P. Pyrolysis kinetics of soybean straw using thermogravimetric analysis. Fuel 2016;169:93–8.
[36] Damartzis T, Vamvuka D, Sfakiotakis S, Zabaniotou A. Thermal degradation studies and kinetic modeling of cardoon (Cynara cardunculus) pyrolysis using thermogravimetric analysis (TGA). Bioresour Technol 2011;102(10):6230–8.
[37] Yuan X, He T, Cao H, Yuan Q. Cattle manure pyrolysis process: Kinetic and thermodynamic analysis with isoconversional methods. Renew Energy 2017;107:489–96.
[38] Asadieraghi M, Wan Daud WMA. Characterization of lignocellulosic biomass thermal degradation and physiochemical structure: Effects of demineralization by diverse acid solutions. Energy Convers Manag 2014;82:71–82.
[39] Arias B, Pevida C, Fermoso J, Plaza MG, Rubiera F, Pis JJ. Influence of torrefaction on the grindability and reactivity of woody biomass. Fuel Process Technol 2008;89(2):169–75.
[40] Bledzki AK, Mamun AA, Volk J. Physical, chemical and surface properties of wheat husk, rye husk and soft wood and their polypropylene composites. Composites Part A: Appl Sci Manufact 2010;41(4):480–8.
[41] Criado JM. Kinetic analysis of DTG data from master curves. Thermochim Acta 1978;24(1):186–9.
[42] Dhyani V, Kumar J, Bhaskar T. Thermal decomposition kinetics of sorghum straw via thermogravimetric analysis. Bioresour Technol 2017;245:1122–9.
[43] Mishra G, Kumar J, Bhaskar T. Kinetic studies on the pyrolysis of pinewood. Bioresour Technol 2015;182:282–8.
[44] Poletto M, Zattera AJ, Santana RMC. Thermal decomposition of wood: Kinetics and degradation mechanisms. Bioresour Technol 2012;126:7–12.
[45] Chen D, Gao A, Ma Z, Fei D, Chang Y, Shen C. In-depth study of rice husk torrefaction: Characterization of solid, liquid and gaseous products, oxygen migration and energy yield. Bioresour Technol 2018;253:148–53.
[46] Chen W-H, Liu S-H, Juang T-T, Tsai C-M, Zhuang Y-Q. Characterization of solid and liquid products from bamboo torrefaction. Appl Energy 2015;160:829–35.
[47] Han Z, Zeng X, Yao C, Xu G. Oxygen Migration in Torrefaction of Eupatorium adenophorum Spreng. and Its Improvement on Fuel Properties. Energy Fuels 2015;29(11):7275–83.
[48] Lu K-M, Lee W-J, Chen W-H, Lin T-C. Thermogravimetric analysis and kinetics of co-pyrolysis of raw/torrefied wood and coal blends. Appl Energy 2013;105:57–65.
[49] Cai J, He Y, Yu X, Banks SW, Yang Y, Zhang X. Review of physicochemical properties and analytical characterization of lignocellulosic biomass. Renew Sustain Energy Rev 2017;76:309–22.
[50] Saikia R, Baruah B, Kalita D, Pant KK, Gogoi N, Kataki R. Pyrolysis and kinetic analysis of a perennial grass (Saccharum ravannae L.) from north-east India: Optimization through response surface methodology and product characterization. Bioresour Technol 2018;253:304–14.
[51] Park J, Meng J, Lim KH, Rojas OJ, Park S. Transformation of lignocellulosic biomass during torrefaction. J Anal Appl Pyrolysis 2013;100:199–206.
[52] Wannapeera J, Fungtammasan B, Worasuwannarak N. Effects of temperature and holding time during torrefaction on the pyrolysis behaviors of woody biomass. J Anal Appl Pyrolysis 2011;92(1):99–105.
[53] Müller-Hagedorn M, Bockhorn H, Krebs L, Müller U. A comparative kinetic study on the pyrolysis of three different wood species. J Anal Appl Pyrolysis 2003;68–69:231–49.
[54] Tong S, Xiao L, Li X, Zhu X, Liu H, Luo G. A gas-pressurized torrefaction method for biomass wastes. Energy Convers Manag 2018;173:29–36.
[55] Doyle CD. Estimating isothermal life from thermogravimetric data. J Appl Polymer Sci 1962;6(24):639–42.
[56] Vamvuka D, Kakaras E, Kastanaki E, Grammelis P. Pyrolysis characteristics and kinetics of biomass residuals mixtures with lignite. Fuel 2003;82(15):1949–60.
[57] Vlaev LT, Markovska IG, Lyubchev LA. Non-isothermal kinetics of pyrolysis of rice husk. Thermochim Acta 2003;406(1):1–7.
[58] Turmanova SC, Genieva SD, Dimitrova AS, Vlaev LT. Non-isothermal degradation kinetics of filled with rise husk ash polypropene composites. Express Polym Lett 2008;2:133–46.
[59] Daugaard DE, Brown RC. Enthalpy for Pyrolysis for Several Types of Biomass. Energy Fuels 2003;17(4):934–9.
[60] Mehmood MA, Ye G, Luo H, Liu C, Malik S, Afzal I. Pyrolysis and kinetic analysis of Camel grass (Cymbopogon schoenanthus) for bioenergy. Bioresour Technol 2017;228:7–24.
[61] Vlaev LT, Georgieva VG, Genieva SD. Products and kinetics of non-isothermal decomposition of vanadium(IV) oxide compounds. J Therm Anal and Calorim 2007;88(3):805–12.
[62] Loy ACM, Gan DKW, Yusup S, Chin BLF, Lam MK, Shahbaz M. Thermogravimetric kinetic modelling of in-situ catalytic pyrolytic conversion of rice husk to bioenergy using rice hull ash catalyst. Bioresour Technol 2018;261:213–22.
[63] Xu Y, Chen B. Investigation of thermodynamic parameters in the pyrolysis conversion of biomass and manure to biochars using thermogravimetric analysis. Bioresour Technol 2013;146:485–93.
[64] Ahmad MS, Mehmood MA, Al Ayed OS, Ye G, Luo H, Ibrahim M, et al. Kinetic analysis and pyrolytic behavior of Para grass (Urochloa mutica) for its bioenergy potential. Bioresour Technol 2017;224:708–13.